
1 **DISCLAIMER: This is a preprint of the paper, i.e. the original version initially. The final version can**
2 **be found by following this link: <https://doi.org/10.1038/s41598-020-79930-7>**

3 Bedload transport in rivers: size matters but so does shape!

4 **Cassel Mathieu*¹, Lavé Jérôme², Recking Alain³, Malavoi Jean-René⁵ and Piégay Hervé¹**

5 ¹ *University of Lyon, CNRS UMR 5600 Environnement Ville et Société, Site ENS de Lyon, 15*
6 *Parvis René Descartes, BP 000F-69342 Lyon Cedex 07, France. casselmathieu@gmail.com*
7 *and herve.piegay@ens-lyon.fr*

8 ³ *CRPG-CNRS, CRPG, Vandœuvre-lès-Nancy, 15, rue Notre Dame des Pauvres BP 20, 54500*
9 *Vandœuvre les Nancy, France. jlave@crpg.cnrs-nancy.fr*

10 ⁴ *Inrae, UR ETNA, Domaine Universitaire, 2 rue de la papeterie BP 76, 38402 Saint-Martin-*
11 *d'Hères, France. alain.recking@inrae.fr*

12 ⁵ *Electricité De France - EDF/DPIH, Département Concessions Eau Environnement*
13 *Territoires. Le PRIMAT - 190 rue Garibaldi, 69003 LYON, France. jean-rene.malavoi@edf.fr*

15 **ABSTRACT**

16 Bedload transport modelling in rivers, which defines the threshold for pebble movement, takes
17 into account the size and density of pebbles, but does not formally consider particle shape. The
18 lack of analyses evaluating the influences of shape and density on particle mobility presents a
19 major deficiency. To address this issue and to compare the relative roles of the density and
20 shape of particles, we performed original sediment transport experiments in an annular flume
21 using molded artificial pebbles equipped with a radio frequency identification tracking system.
22 The particles were designed with four distinct shapes and four different densities while having
23 the same volume, and their speeds and distances traveled under constant hydraulic conditions
24 were analyzed. The results show that particle shape has more influence than particle density on
25 the resting time between particle displacement and the mean traveling distance. For all densities
26 investigated, the particle shape systematically induced differences in travel distance that were
27 strongly correlated ($R^2 = 0.94$) with the Sneed and Folks shape index. Such shape influences,

28 although often mentioned, are here quantified for the first time, demonstrating why and how
29 they can be included in bedload transport models.

30

31 INTRODUCTION

32 Sediment transport is a key process in fluvial geomorphology, being important for
33 sustainable management of navigable channels, designing engineering projects, predicting
34 morphological changes and associated hydraulic risks, interpreting sedimentary archives and
35 restoring rivers ¹. It involves three phases of particle mobility: (1) entrainment ²⁻⁶; (2) motion
36 ⁷⁻⁹; and (3) deposition ^{10,11}. Sediment transport at the particle scale is a stochastic phenomenon
37 ^{7,12,8,13,14,9}, which mostly arises from the complex interactions between particle collisions and
38 highly variable friction, drag, and lift forces due to fluid turbulence. Thus, for practical
39 considerations, empirically calibrated sediment transport functions widely use Shields stress
40 number (τ^* or θ) to quantify the balance of the forces exerted on the channel bed particles, and
41 the critical Shields number (τ^*_c), which is the threshold value necessary to set particles in
42 motion, to determine the moments at which drag forces exceed stabilizing forces ($\tau^* > \tau^*_c$) and
43 particles can be entrained ¹⁵⁻²¹. Such approaches have been used to estimate particle stabilizing
44 forces from median pebble size and submerged density ¹⁶. At the river reach scale, sediment
45 transport estimates generally encapsulate a relation depending on the Shields stress, and
46 therefore also include the median grain size ^{20,22-27} of the transported sediment.

47 Published bedload transport datasets from rivers with similar flow conditions,
48 morphologies, and median grain sizes, may show different transport rates, with large variations
49 in the threshold for setting particles in motion ²⁸, variations that can be up to 10-fold ²⁹ around
50 the mean empirical Shields curve ³⁰⁻³². To explain such dispersion, many studies have focused
51 on the role of mixed grain size, hiding effects ³³⁻³⁶, macro-roughness, channel steepness, or bed
52 roughness relative to channel depth ³⁷. However, fewer studies have qualitatively related pebble

53 shape to bedload transport through the influence of pebble angularity^{38,39}, pebble imbrication
54^{34,35,40}, or bed roughness^{34,40,41} (i.e. the D/K ratio, where D is the diameter of the particles to be
55 moved and K is the bed-particle diameter). In environments with smooth-beds ($D > K$) and
56 during low to moderate flood events, coarse particles of spherical or ellipsoid shape were
57 observed⁴² to be more likely to experience entrainment and transport than flatter shapes.
58 Conversely, in rough-bed rivers ($D < K$), Demir and Walsh¹ found that displacement of flatter
59 shapes (i.e. discs and blades) seems to be promoted. Overall, selective shape entrainment and
60 travel length both decrease as flood magnitude increases and/or particle size decreases⁴³.
61 Whereas these previous studies have emphasized that robust deterministic expression of initial
62 motion should encapsulate the role of particle shape and bed roughness in particle motion
63 modelling^{38,39,44,45}, the scarcity of field and experimental data has prevented a quantitative
64 account of this role.

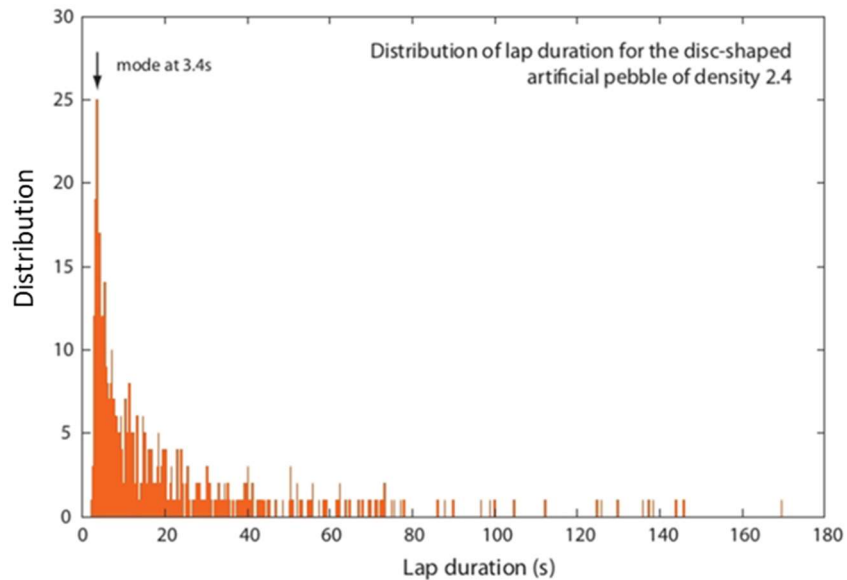
65 To partially fill this gap, we designed a parametric study based on experiments run in
66 an annular flume in which the displacements (encapsulating onset motion, travel length and rest
67 periods) of artificial pebbles of various shapes and densities were tracked for several hours.
68 Particle shape has been quantified by many different parametrizations⁴⁶⁻⁵² expressing
69 angularity, surface roughness, or departure from sphericity. As the latter directly impacts on
70 inertial moments and pivoting angle, we investigated the influence of shape in terms of the
71 departure from sphericity, examining various ellipsoid particle shapes (from plate to blade
72 types).

73

74 **RESULTS**

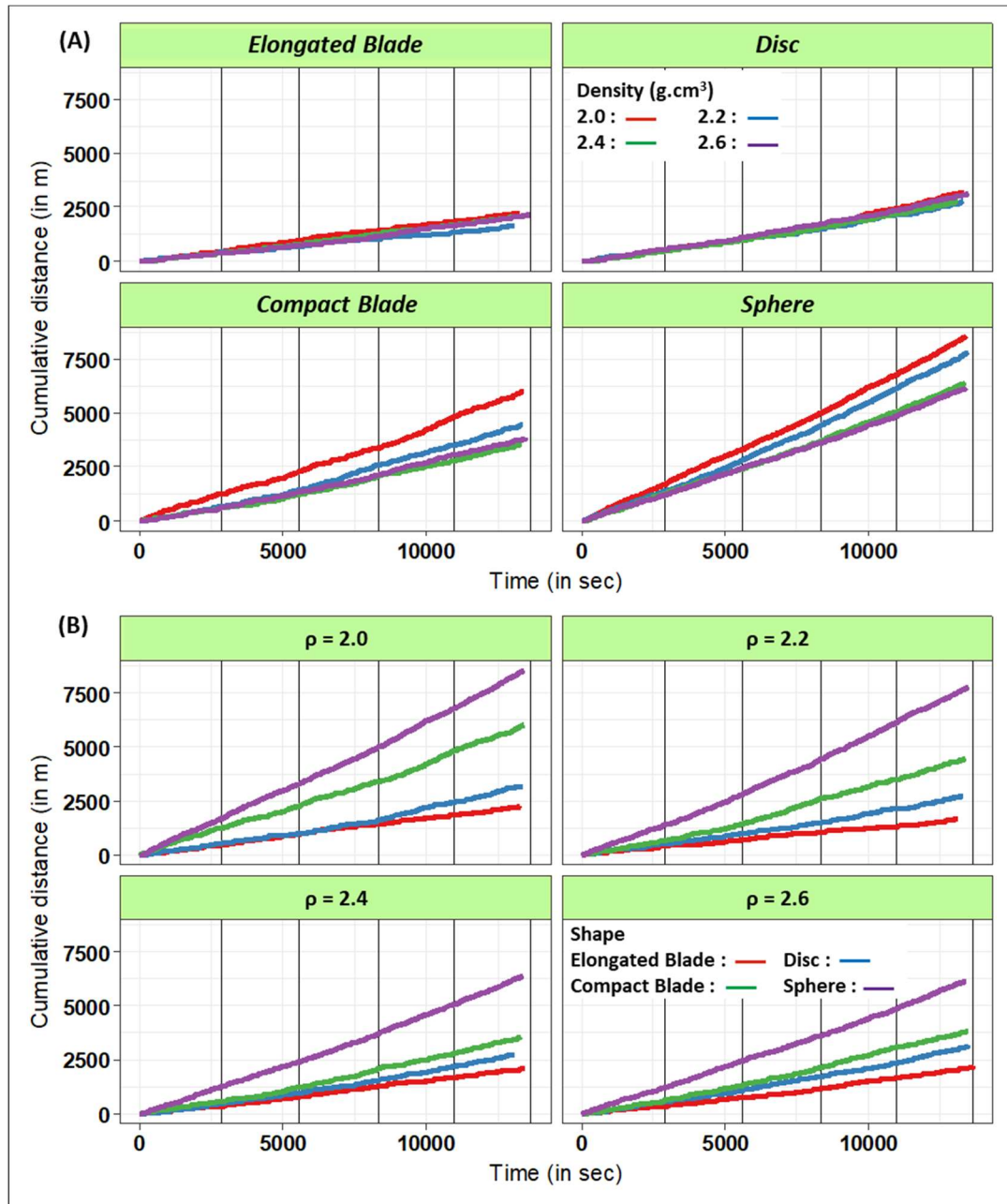
75 The number of revolutions made by the monitored particles ranged between 439 laps
76 for an elongated blade and 2270 laps for a sphere, making the lap duration observations were
77 taken from large sample sizes. Although the lap durations within the annular flume displayed

78 large variations (from 3 seconds up to a few minutes; see example in Figure 1) over the total
79 run duration, the cumulative travel distances of the particles (Figure 2) displayed a fairly
80 constant slope that permitted the average traveling velocities of the different artificial pebbles
81 to be defined.



82
83 **Figure 1. Example of the distribution of lap durations (shape = disc; density = 2.4 g.cm⁻³)**

84 The slight increases observed in the slopes of the cumulative distance curves over time
85 for all shapes and densities reflect the progressive augmentation of the particles' velocities
86 caused by a decrease in the mixing load due to abrasion (relative mass loss of 1.2% per
87 kilometer traveled). As this was moderate and affected all tagged particles in a similar manner,
88 we consider that it had very little impact on the first-order estimates and results of the
89 experiments.



90
91 **Figure 2. Cumulative travel distances over time according to particle shape (A) and**
92 **density (B).**

93 The four particle shapes investigated exhibited clear differences in cumulative travel
94 length, with variations in the particle densities also demonstrating effects (Figure 2). The
95 spherical particles traveled the farthest and fastest (mean velocities ranging from 0.44 to 0.60
96 m.s⁻¹), with their mean virtual velocities displaying an inverse relationship with density (Figure
97 3). The compact blade-shaped particles were the second fastest, exhibiting mean velocities
98 ranging from 0.25 to 0.44 m.s⁻¹, again displaying an inverse relationship with density, although

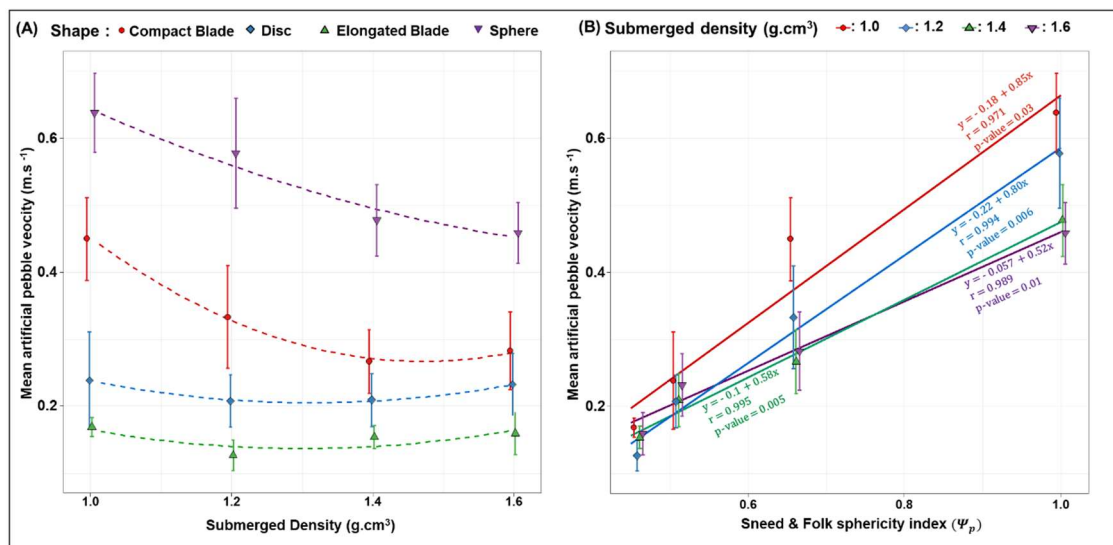
99 to a lesser extent than that of the spherical particles. In contrast, the mean virtual velocities of
 100 the disc- and elongated blade-shaped particles were minimally influenced by their densities: the
 101 mean velocities were clustered within a narrow range from 0.14 to 0.17 m.s⁻¹ and 0.19 to 0.21
 102 m.s⁻¹ respectively. Within the density classes, the distances traveled by the particles clearly
 103 showed a high variability in relation to their shapes (Figure 2B and Figure 3A). The experiments
 104 clearly indicate that the variability in velocity associated with pebble shape is substantially
 105 higher than that associated with particle density (~100% compared with ~30%).

106 To explore the influence of particle shape on mobility in a more quantitative way, we
 107 used the sphericity index, Ψ_p (1), of Sneed and Folks (1958):

$$108 \quad \Psi_p = \sqrt[3]{\frac{S^2}{LI}} \quad \text{Equation (1)}$$

109 where L , I , and S are the longest, intermediate, and shortest axes of the pebbles.

110 The sphericity index Ψ_p shows a remarkable positive relationship with the mean
 111 traveling velocity (Figure 3B). Moreover, the mean velocities increased from 0.52 to 0.85 m.s⁻¹
 112 ¹ for decreasing densities from 2.6 to 2.0 g.cm⁻³. These results suggest that it is possible to
 113 estimate differences in the mean virtual velocities and mobilities of particles according to their
 114 sphericity.

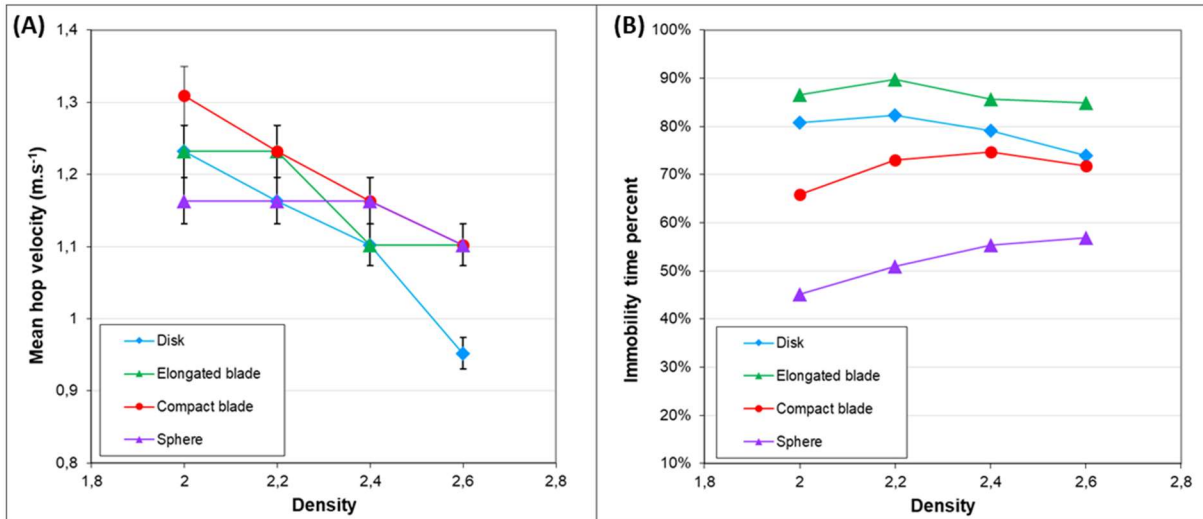


115
 116 **Figure 3. Mean velocity as function of density (A) and Sneed and Folk spherical index (B).**

117 The lap-scaled average travel velocities measured integrate the duration of motion
118 phases and the resting periods in between. However, the pebble shape and density can
119 potentially impact each of these two phases differently. The lap duration distributions are
120 characterized by a first peak at around 3 s in all experiments (Figure 1), which corresponds to
121 a revolution speed of $\sim 1.2 \text{ m}\cdot\text{s}^{-1}$. For experimental conditions similar to those used in this study,
122 high speed camera viewing⁵⁶ previously indicated a mean hop velocity of $1.2 \pm 0.2 \text{ m}\cdot\text{s}^{-1}$ for
123 pebbles in an annular flume. This modal lap duration of ~ 3 s therefore represents a continuous
124 succession of hops over a full lap, without any resting time. These modal values decrease
125 slightly with increasing density (Figure 4A), as expected from the larger inertial effects after
126 the pebble is set in motion. More importantly, they are almost independent of the pebble shape,
127 as was also observed in a straight flume study⁶³. This implies that the impact of shape on the
128 mean traveled distance is mostly caused by its influence on the resting time between
129 movements, i.e. on the immobilization conditions and on the threshold for setting pebbles in
130 motion. To illustrate this inference, a simple calculation of the mean resting time fraction, or
131 immobility ratio (I_r), can be estimated through

$$I_r = \frac{T - N_l t_m}{T} \quad , \quad \text{Equation (1)}$$

132 with T being the total duration of the runs, N_l the number of achieved flume revolutions during
133 T , and t_m the modal lap duration (first mode on the distribution of Figure 1) corresponding to a
134 continuous succession of hops over a full lap.
135



136
 137 **Figure 4. (A) mean hop velocity and (B) time fraction of immobility of the 16 different**
 138 **artificial pebbles.**

139 Except for spherical pebbles that display a slight increase, the immobility ratio (Figure
 140 4B) is only weakly or not affected by the particle density. In contrast, the shape of a pebble
 141 deeply impacts its mobility, with the immobility ratio raging from ~50% for the spherical
 142 shapes up to $\geq 85\%$ for the elongated blades.

143
 144 **DISCUSSION**

145 The greater velocity of the spherical and compact-blade-shaped particles relative to the
 146 elongated-blade and disc-shaped particles is in good accordance with the literature^{1,39,64}, given
 147 that the flatness of the flume bottom constitutes a low roughness bed surface, despite clustering
 148 of temporary resting pebbles. As most lithologies of the pebbles present in rivers show a density
 149 close to 2.7 g.cm^{-3} , very similar to the highest value used in this study, we expect their mean
 150 velocities to be more strongly influenced by their shape than by their density. On a quantitative
 151 basis, this supports the claimed need to include a particle shape parameter in the sediment
 152 transport equation^{34,41,65}.

153 To do this, we focus on the conditions for setting a particle in motion, because pebble
 154 shape has a major influence on virtual velocity through resting periods. Following Komar and

155 Li's (1986)⁴¹ description, balancing of the moments of tractive and resisting forces for the
 156 critical stress yields:

$$157 \quad \tau_c \propto \frac{l_w \Delta \rho g S I L}{l_D A_a} \quad \text{Equation (2)}$$

158 where A_a is the apparent section exposed to the flow, and l_D and l_w the respective moment
 159 arms of the drag force and submerged weight respectively. Assuming that pebbles tend to lie
 160 with their S -axis vertically oriented, the moment arms of the drag force l_D approximately scales
 161 with the S -axis. As a pebble can orient either longitudinally or transversally, we use the
 162 intermediate variable \sqrt{LI} to account for the apparent section exposed to the flow ($A_a \propto S\sqrt{LI}$)
 163 and the moment arm of the submerged weight l_w . Therefore:

$$164 \quad \tau_c \cong k \frac{\sqrt{LI} \Delta \rho g^3 \sqrt{(SIL)^2 \tilde{D}}}{S^2 \sqrt{LI}} = k^3 \sqrt{\frac{(LI)^2}{S^4}} \Delta \rho g \tilde{D} = k \frac{1}{\Psi_p^2} \Delta \rho g \tilde{D} \quad \text{Equation (3)}$$

165 where k is a function of the particles' Reynold number considered as a constant, $\tilde{D} =$
 166 $\sqrt[3]{SIL}$, the mean pebble size, and $\Psi_p = \sqrt[3]{\frac{S^2}{LI}}$, the Sneed and Folk's index. Here, $\frac{1}{\Psi_p^2}$ corresponds
 167 more or less to the term $\tan \phi$ in Komar and Li (1986): when particle flatness increases (i.e.
 168 Ψ_p decreases), the pivoting angle increases and mobility is reduced. Suppressing the unknown
 169 k , the threshold can be expressed as:

$$170 \quad \tau_c \cong \left(\frac{\Delta \rho}{\Delta \rho_{ref}} \right) \left(\frac{\Psi_{p_{ref}}}{\Psi_p} \right)^2 \tau_{c_{ref}} \quad \text{Equation (4)}$$

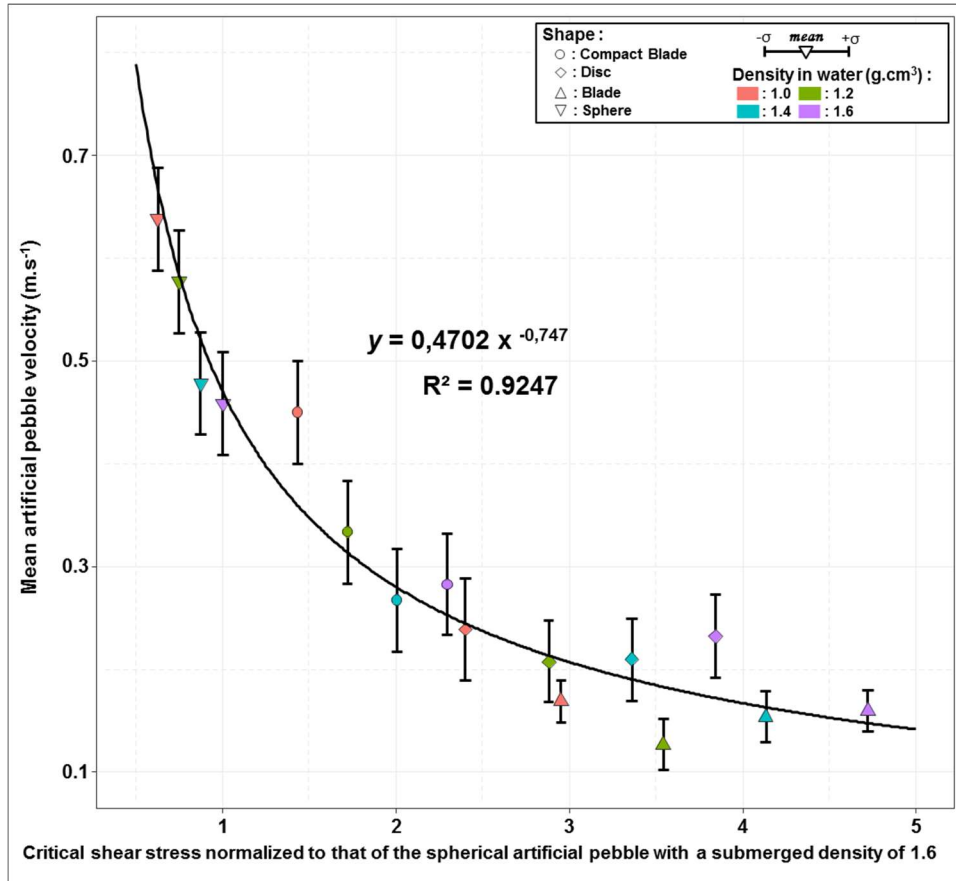
171 where $\tau_{c_{ref}}$ is the critical Shields stress of a reference pebble of similar size.

172 The non-dimensional critical threshold is expressed as:

$$173 \quad \tau_c^* \cong \frac{\tau_c}{\Delta \rho g} = \frac{k}{\Psi_p^2} = \left(\frac{\Psi_{p_{ref}}}{\Psi_p} \right)^2 \tau_{c_{ref}}^* \quad \text{Equation (5)}$$

174 where $\tau_{c_{ref}}^*$ is the critical Shields stress of a reference pebble of similar size.

175 Representing the mean travel velocity of the particle as a function of the critical stress
 176 τ_c shows an inverse trend between the two variables (Figure 5): both density and departure from
 177 sphericity decrease the ratio of tractive over resistive moments and favor particle immobility.



178
 179 **Figure 5. Mean velocity of the 16 artificial pebbles vs. their critical shear stress normalized**
 180 **to that of the spherical artificial pebble with a submerged density of 1.6** ($= \frac{\tau_c}{\tau_{c_{ref}}} = \left(\frac{\Delta\rho}{1.6}\right) \left(\frac{1}{\Psi_p}\right)^2$).

181 Most bedload transport capacity formulae are functions of the excess Shields stress and
 182 follow two general forms: (1) $\Phi = K(\tau^* - \tau_c^*)^\alpha$, and (2) $W^* = (\tau/\tau_c)^\alpha$, where Φ and W^* are two
 183 distinct non-dimensional expressions of the bedload transport rate, and α and K two constant
 184 terms⁶⁶. To account for the role of pebble shape in a transport capacity relationship, one could
 185 introduce into the formula the modified expression for critical shear stress (eq. 4), or the critical
 186 Shields stress (eq. 5) that includes the Sneed and Folk Index.

187 To explore this hypothesis, we built on the fractional transport rate model developed for
 188 transport of a mixture of grain sizes (e.g. Parker et al., 1982⁶⁷). This choice was motivated by
 189 the fact that such a relation already proposes a similarity collapse for heterogeneous sediment,
 190 which is the case in our experiments with particles of variable shapes and densities mixed with
 191 a natural pebble load. We arbitrarily considered Wilcock and Crowe's (2003)⁶⁸ relation for
 192 fractional transport rate, in which the form of the similarity collapse is:

$$193 \quad W_i^* = 14 \left(1 - \frac{0.894}{\phi^{0.5}}\right)^{4.5} \quad \text{when } \phi = \frac{\tau}{\tau_{ci}} \geq 1.35 \quad \text{Equation (6)}$$

194 where τ is the bed shear stress, τ_{ci} the critical shear stress for incipient motion of a specific
 195 pebble i (more exactly it corresponds to the minimum shear stress required to achieve a small
 196 reference transport rate of $W_i^* = 0.002$ ⁶⁷), and W_i^* the dimensionless transport rate $W_i^* =$
 197 $\frac{Rgq_{bi}}{F_i\left(\frac{\tau}{\rho}\right)^{3/2}}$, with $R_i = \frac{\Delta\rho_i}{\rho}$ being the ratio of the submerged sediment (of type i) density to water
 198 density, g being gravity, q_{bi} the volumetric transport rate per unit width of the particle of type i
 199 (i.e. of similar shape, size, and density), and F_i the proportion of the pebble type being of the
 200 class i .

201 Following our simplified analysis of the force moment balance, we defined the critical
 202 (or reference) shear stress as a function (eq. 7) of the mean characteristics of the transported
 203 sediment load (i.e. mean gravel size D_m , mean shape factor Ψ_{Pm} , and mean density $\Delta\rho_m$)
 204 according to:

$$205 \quad \tau_{ci} = \left(\frac{\Delta\rho_i}{\Delta\rho_m}\right) \left(\frac{\Psi_{Pm}}{\Psi_{Pi}}\right)^2 \tau_{cm} \quad \text{Equation (7)}$$

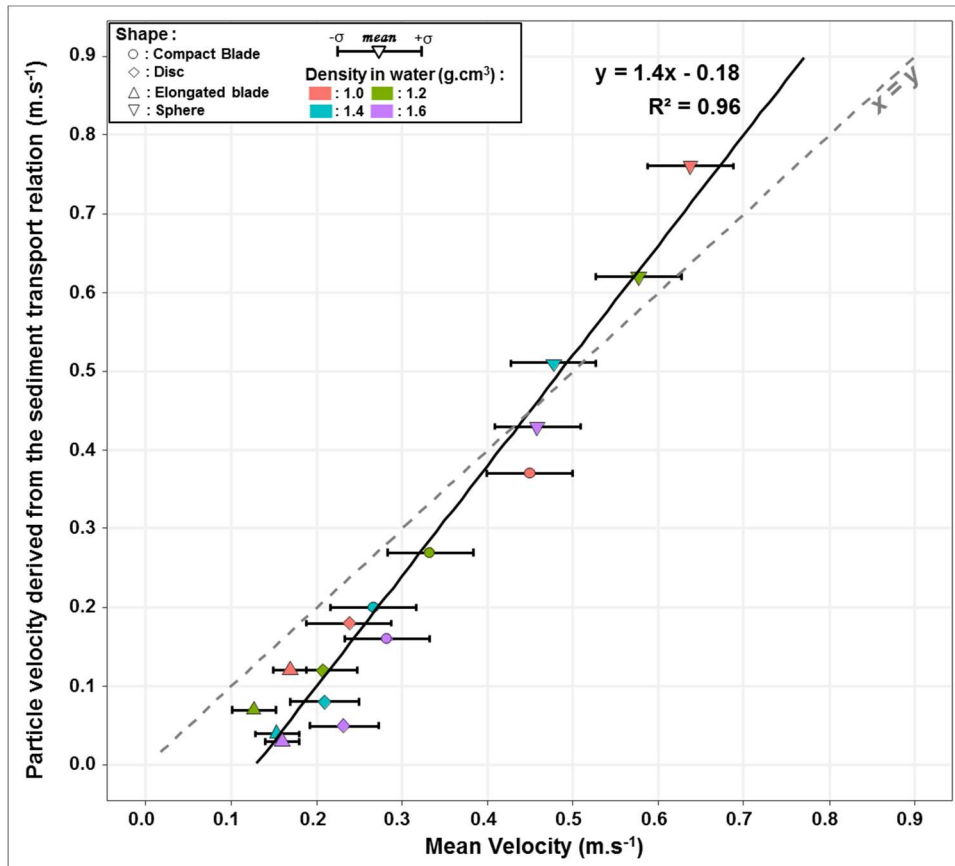
206 with τ_{cm} being the critical shear stress for the mean gravel load. Here,
 207 $\tau_{cm} = \Delta\rho_m g D_m \tau_c^* \cong 28 \text{ Pa}$ considering that $\Delta\rho = 2600 \text{ kg.m}^{-3}$, $D_m \approx 5 \text{ cm}$ for the mean
 208 gravel diameter of the 65 kg of limestone pebbles, and $\tau_c^* \cong 0.036$ ⁶⁸.

209 Within the flume, provided that not all of the particles are in full motion, the conditions
 210 of alluvial rivers prevail, i.e. the sediment flux q_{si} is equated by the transport capacity q_{bi} . In our
 211 experiments, the mass sediment flux per unit width of the pebble class i can be expressed from
 212 the mean traveling velocity through: $q_{si} = \frac{F_i M}{A} V_{gi}$, with A being the surface of the flume
 213 bottom, M the mass of sediment introduced into the flume, and V_{gi} the mean displacement
 214 velocity of particles of type i . It follows that a virtual mean velocity can be derived for particle
 215 i from the above fractional transport rate equation:

$$216 \quad V_{gi} = \frac{AM\rho_{si}}{R_i g} \left(\frac{\tau}{\rho}\right)^{3/2} W_i^* \left(\frac{\tau}{\tau_{ci}}\right) \quad \text{Equation (8)}$$

217 with τ_{ci} derived from equation (7) and a mean shape factor $\Psi_{pm} = 0.7 \pm -0.08$ for the 65 kg
 218 of limestone pebbles.

219 The virtual velocities derived from the bedload transport relation show a well-defined
 220 correlation with the measured virtual velocities (Figure 6). However, the slope of the correlation
 221 line is larger than unity, and our modified version of the bedload transport tends to
 222 underestimate the observed transport for the densest elongated-blade or disk-shaped pebbles.
 223 Despite these slight discrepancies from the observations, these results suggest that the role of
 224 pebble shape on bedload transport can be predicted, and that the inclusion of pebble shape
 225 characteristics in the modelling of bedload transport offer much promise for improving bedload
 226 transport predictions.



227

228 **Figure 6. Comparison between the mean measured velocities of particles of various shapes**
 229 **and densities and the theoretical particle velocity derived from a fractional transport rate**
 230 **relation adapted from Wilcock and Crowe's (2003) relation ⁶⁸.**

231 In terms of sediment dynamics, pebbles travel in the flume following an alternating
 232 pattern of resting and motion periods, as generally observed in a natural stream⁸. We therefore
 233 consider that our experiments succeeded in capturing the first order behavior of the bedload,
 234 and that the introduction of a shape factor into critical Shield stress and bedload transport
 235 models might be transposed to rivers. However, the experimental conditions are slightly distinct
 236 from those of natural rivers, in particular the use of a monodispersed sediment load and a low-
 237 roughness bottom. Additional experiments exploring distinct bottom conditions, grain size
 238 distributions, and using straight channels are probably necessary to strengthen our initial results
 239 and resolve the slight discrepancies between the model and observations. Similarly,
 240 experiments using pebbles with a unique and defined type of particle shape (for example, only

241 platy particles, as expected in sediment derived from the erosion of schist-rich lithologies),
242 instead of a single particle mixed with a large population of pebbles of distinct shapes, should
243 help to derive a more universal relationship. Nevertheless, this study represents a preliminary
244 and promising step towards addressing the role of particle shape in bedload transport.

245

246 CONCLUSION

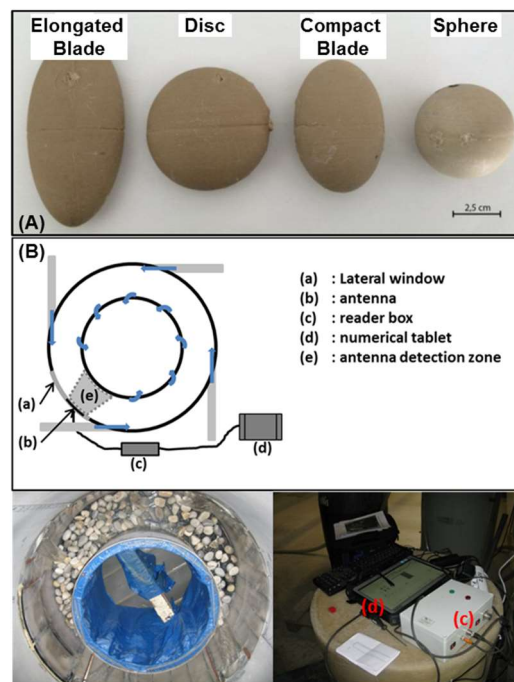
247 These experiments, based on innovative tools (artificial pebbles of controlled density
248 containing RFIDs) offer new perspectives for studying sediment transport mechanisms. The
249 comparative analysis of the shape and density of particles on their mobility highlights the
250 crucial influence of particle shape. Furthermore, it also indicates that the sphericity index (Ψ_p)
251 of Sneed and Folks (1958)⁶⁹, which correlates with mean velocity, is relevant for including
252 shape parameters in sediment transport formulae. The method developed in this study can be
253 reproduced to investigate how bed roughness (changing D/K ratio) and/or a tracer's grain-size
254 can change the balance between the effects of shape and density on particle velocity. It allows
255 investigation of whether bed roughness promotes the transport of flat-shaped particles, as
256 reported in the literature, and whether particle density can mitigate this effect. Repeating the
257 experiments with smaller particle sizes (maintaining a constant D/K ratio) would also allow
258 investigation of whether size mitigates the influence of shape and density on particle transport.

259

260 METHODS

261 We designed four differently-shaped particle models within the grain-size class of 45–
262 64 mm (5.5–6.0 Ψ -units), with all models having the same volume (*i.e.* 49.3 cm³) but exhibiting
263 differences in the sphericity index ⁵³ (Figure 7A ; Table 1). After creating silicon molds (RTV
264 120) for these four models, we manufactured 16 artificial pebbles using a mixture of resin and
265 corundum powder in variable proportions, creating pebbles of four different densities (2.0, 2.2,

266 2.4, and 2.6 g.cm⁻³) for each mold shape ⁵⁴. We equipped these artificial pebbles with
 267 transponders of Radio Frequency Identification, RFID, (model RI-TRP-WR2B of Texas
 268 Instrument, Dallas Texas USA, also known as PIT Tags) to monitor their displacements within
 269 an annular flume⁵⁵ (Figure 7B). A detection antenna located on the outside of the flume, along
 270 a lateral window, enabled tracking of the number of laps achieved by the RFID-equipped
 271 pebbles and the time for each revolution.



272 *Figure 7. The four particle shapes investigated (A) and the*
 273 *annular flume equipped with the RFID system (B).*
 274

275

276 **Table 1. Shape characteristics of the artificial particles tracked in the flume.**

SHAPE	<i>a</i> -axis (mm) <i>L</i>	<i>b</i> -axis (mm) <i>I</i>	<i>c</i> -axis (mm) <i>S</i>	Vol.(cm ³)	Sphericity index (Sneed and Folks, 1958)
Compact Blade	68.1	46	30	49.3	0.66
Sphere	45.5	45.5	45.5	49.3	1
Disc	65	63	23	49.3	0.51
Elongated Blade	97.2	46.1	21	49.3	0.46

277

278 In an attempt to reproduce bedload transport conditions, these artificial pebbles were
279 mixed with 65 kg of limestone pebbles of a similar grain-size (i.e. class 45–64 mm) and were
280 run within an annular flume⁵⁶. A set of experiments were run following the designs of previous
281 studies^{54,56,57} for which the sediment dynamics have been characterized⁵⁶, i.e. with a low
282 roughness bottom and a monodispersed grain size distribution. During the experiments, the
283 pump discharge sustaining the fluid injection into the flume was maintained at 240 m³.h⁻¹,
284 which for the introduced sediment mass corresponds⁵⁶ to a shear stress of $\tau = 135$ Pa at the base
285 of the flume according to Euler theorem applied to the moments, a Shield stress of $\tau^* = 0.16$, a
286 mean transit velocity for pebbles of ≈ 0.4 m.s⁻¹, and a sediment flux of ~ 24 kg.m⁻¹.s⁻¹. Under
287 these conditions, high speed camera viewing⁵⁶ indicated that the pebbles were transported in
288 the annular flume in a similar manner to that observed⁸ in rivers, with alternating transport
289 phases with rolling and saltation, and resting times caused by temporary blockage and piling of
290 particles.

291 Each experimental run lasted for 45 minutes. To avoid superpositioning of radio-
292 frequency signals and missed RFID transponder detections^{54,58,59}, only the four particles of the
293 same density were simultaneously present in the flume, thereby also limiting to four the number
294 of transponders. A total of six runs were achieved for the densities of 2.6 and 2.4 g.cm⁻³, and
295 five runs for the densities of 2.0 and 2.2 g.cm⁻³. For each artificial pebble, the combined runs
296 provide a long duration of almost 4 hours and a large cumulative traveled distance, from which
297 the mean traveled velocity (or virtual velocity as defined by Haschenburger and Church⁶⁰) can
298 be computed and the distributions of the lap times estimated. Finally, we compared the virtual
299 velocities and lap distributions of the 16 artificial pebbles, to investigate the effects of the
300 different shapes and densities on bedload transport. In this study, the use of an annular flume
301 enabled the acquisition of a relatively long time series compared with typical straight flume
302 experiments⁶¹ and the sampling of a population of practically uncensored particle trajectories

303 without the limitations induced by a limited detection window or flume length⁶². This ensured
304 that the ranges of traveled distances under conditions of continuous movement were well
305 represented in the experiment. We also made sure that the duration of the experiments (45
306 minutes) was much longer than the maximum resting time recorded (~5 minutes), to avoid time
307 censorship effects on the distributions of the resting periods and lap times, and to be sure of the
308 statistical significance of the distributions.

309

310

311

312

313

314

315

316

317

318

319

320

321

322

323

324

325

326

327

328 **References:**

- 329 1. Demir, T. & Walsh, R. P. D. Shape and size characteristics of bedload transported during winter
330 storm events in the Cwm Treweryn Stream, Brecon Beacons, South Wales. *Turk. J. Earth Sci.* **14**,
331 105–121 (2005).
- 332 2. Mears, A. I. Flooding and sediment transport in a small alpine drainage basin in Colorado.
333 *Geology* **7**, 53 (1979).
- 334 3. Bradley, W. C. & Mears, A. I. Calculations of Flows Needed to Transport Coarse Fraction of
335 Boulder Creek Alluvium at Boulder, Colorado. *Geol. Soc. Am. Bull.* **91**, 1057–1090 (1980).
- 336 4. Einstein, H. A. & El-Samni, E.-S. A. Hydrodynamic Forces on a Rough Wall. *Rev. Mod. Phys.* **21**,
337 520–524 (1949).
- 338 5. Cheng, E. D. H. & Clyde, C. G. Instantaneous hydrodynamic lift and drag forces on large
339 roughness elements in turbulent open channel flow. in 3-1-3–20 (H. W. Shen, 1972).
- 340 6. Komar, P. D. & Li, Z. Applications of grain-pivoting and sliding analyses to selective entrapment of
341 gravel and to flow-competence evaluations. *Sedimentology* **35**, 681–695 (1988).
- 342 7. Einstein, H. Bed load transport as a probability problem. 1–105 (1937).
- 343 8. Habersack, H. M. Radio-tracking gravel particles in a large braided river in New Zealand: A field
344 test of the stochastic theory of bed load transport proposed by Einstein. *Hydrol. Process.* **15**,
345 377–391 (2001).
- 346 9. Olinde, L. & Johnson, J. Using RFID and accelerometer-embedded tracers to measure
347 probabilities of bed load transport, step lengths, and rest times in a mountain stream. *Water*
348 *Resour Res* **51**, 7572–7589 (2015).
- 349 10. Hjulström, F. Studies of the morphological activity of rivers as illustrated by the River Fyris.
350 Inaugural dissertation,. (Almqvist & Wiksells, 1935).
- 351 11. Einstein, A. H. Bedload transport as a probability problem. (Colorado State University, 1937).

- 352 12. Ergenzinger, P. & Schmidt, K. H. Stochastic elements of bed load transport in a steppool
353 mountain river. *Hydrol. Mt. Reg. II—Artificial Reserv. Water Slopes Int. Assoc. Hydrol. Sci. Publ.*
354 **194**, 39–46 (1990).
- 355 13. Busskamp, R. The influence of channel steps on coarse bed load transport in mountain torrents:
356 case study using the radio tracer technique ‘PETSU’. in *Dynamics and geomorphology of*
357 *mountain rivers* 129–139 (Springer, 1994).
- 358 14. Olinde, L. Displacement and entrainment behavior of bedload clasts in mountain streams.
359 (University of Texas, 2015).
- 360 15. Shields, A. Application of similarity principles and turbulence research to bed-load movement.
361 *CalTech Libr.* (1936).
- 362 16. Meyer-Peter, E. & Müller, R. Formulas for Bed-Load transport. *IAHSR 2nd Meet. Stockh. Append.*
363 **2** (1948).
- 364 17. Engelund, F. & Hansen, E. A monograph on sediment transport in alluvial streams. *Tech. Univ.*
365 *Den. Ostervoldgade 10 Cph. K* (1967).
- 366 18. Ackers, P. & White, W. R. Sediment Transport: New Approach and Analysis. *J. Hydraul. Div.* **99**,
367 2041–2060 (1973).
- 368 19. Parker, G. & Klingeman, P. C. On why gravel bed streams are paved. *Water Resour. Res.* **18**,
369 1409–1423 (1982).
- 370 20. Recking, A., Frey, P., Paquier, A., Belleudy, P. & Champagne, J. Y. Feedback between bed load
371 transport and flow resistance in gravel and cobble bed rivers: FEEDBACK BETWEEN BED LOAD
372 AND FLOW RESISTANCE. *Water Resour. Res.* **44**, (2008).
- 373 21. Piton, G. & Recking, A. The concept of travelling bedload and its consequences for bedload
374 computation in mountain streams: HOW TO ACCOUNT FOR ALLOGENIC SUPPLY IN BEDLOAD
375 TRANSPORT EQUATIONS? *Earth Surf. Process. Landf.* (2017) doi:10.1002/esp.4105.
- 376 22. Rickenmann, D. Hyperconcentrated Flow and Sediment Transport at Steep Slopes. *J. Hydraul.*
377 *Eng.* **117**, 1419–1439 (1991).

- 378 23. Smart, G. & Jäggi, M. *Sediment transport on steep slopes. Mitteilung. 64. Versuchsanstalt für*
379 *Wasserbau, Hydrologie und Glaziologie.* (ETH Zurich, Zurich, 1983).
- 380 24. Parker, G., Klingeman, P. C. & McLean, D. G. Bedload and Size Distribution in Paved Gravel-Bed
381 Streams. *J. Hydraul. Div.* **108**, 544–571 (1982).
- 382 25. Wilcock, P. R. & Crowe, J. C. Surface-based Transport Model for Mixed-Size Sediment. *J. Hydraul.*
383 *Eng.* **129**, 120–128 (2003).
- 384 26. van Rijn, L. C. Sediment Transport, Part I: Bed Load Transport. *J. Hydraul. Eng.* **110**, 1431–1456
385 (1984).
- 386 27. Recking, A. Theoretical development on the effects of changing flow hydraulics on incipient bed
387 load motion: INCIPIENT MOTION CONDITIONS. *Water Resour. Res.* **45**, (2009).
- 388 28. Frey, P. & Church, M. How River Beds Move. *Science* **325**, 1509–1510 (2009).
- 389 29. Buffington, J. M. & Montgomery, D. R. A systematic analysis of eight decades of incipient motion
390 studies, with special reference to gravel-bedded rivers. *Water Resour. Res.* **33**, 1993–2029
391 (1997).
- 392 30. Gessler, J. *Chapter 7 Preprint of Paper Beginning and Ceasing of Sediment Motion.* (Colorado
393 State University, 1970).
- 394 31. Miller, M. C., McCAYE, I. N. & Komar, P. D. Threshold of sediment motion under unidirectional
395 currents. *Sedimentology* **24**, 507–527 (1977).
- 396 32. Yalin, M. S. & Silva, A. M. F. da. *Fluvial processes.* (IAHR, 2001).
- 397 33. Miller, R. L. & Byrne, R. J. The angle of repose for a single grain on a fixed rough bed.
398 *Sedimentology* **6**, 303–314 (1966).
- 399 34. Li, Z. & Komar, P. D. Laboratory measurements of pivoting angles for applications to selective
400 entrainment of gravel in a current. *Sedimentology* **33**, 413–423 (1986).
- 401 35. Kirchner, J. W., Dietrich, W. E., Iseya, F. & Ikeda, H. The variability of critical shear stress, friction
402 angle, and grain protrusion in water-worked sediments. *Sedimentology* **37**, 647–672 (1990).

- 403 36. Buffington, J. M., Dietrich, W. E. & Kirchner, J. W. Friction angle measurements on a naturally
404 formed gravel streambed: Implications for critical boundary shear stress. *Water Resour. Res.* **28**,
405 411–425 (1992).
- 406 37. Lamb, M. P., Brun, F. & Fuller, B. M. Hydrodynamics of steep streams with planar coarse-grained
407 beds: Turbulence, flow resistance, and implications for sediment transport: HYDRODYNAMICS OF
408 STEEP STREAMS. *Water Resour. Res.* **53**, 2240–2263 (2017).
- 409 38. Miller, R. L. & Byrne, R. J. The Angle of Repose for a Single Grain on a Fixed Rough Bed.
410 *Sedimentology* **6**, 303–314 (1966).
- 411 39. Carling, P. A., Kelsey, A. & Glaister, M. S. Effect of bed roughness, particle shape and orientation
412 on initial motion criteria. in *Dynamics of Gravel-bed Rivers* 24–39 (Hey, R.D. Billi, P., Thorne, C.R.
413 and Tacconi, P. (eds), 1992).
- 414 40. Lane, E. W. & Carlson, E. J. Some observations on the effect of particle shape on the movement
415 of coarse sediments. *Eos Trans. Am. Geophys. Union* **35**, 453–462 (1954).
- 416 41. Komar, P. D. & Li, Z. Pivoting analyses of the selective entrainment of sediments by shape and
417 size with application to gravel threshold. *Sedimentology* **33**, 425–436 (1986).
- 418 42. Schmidt, K.-H. & Ergenzinger, P. Bedload entrainment, travel lengths, step lengths, rest periods—
419 studied with passive (iron, magnetic) and active (radio) tracer techniques. *Earth Surf. Process.*
420 *Landf.* **17**, 147–165 (1992).
- 421 43. Schmidt, K.-H. & Gintz, D. Results of Bed load tracer experiments in a mountain river. in *River*
422 *Geomorphology* 37–54 (Wiley, 1995).
- 423 44. Buffington, J. M., Dietrich, W. E. & Kirchner, J. W. Friction angle measurements on a naturally
424 formed gravel streambed: Implications for critical boundary shear stress. *Water Resour. Res.* **28**,
425 411–425 (1992).
- 426 45. White, C. M. The Equilibrium of Grains on the Bed of a Stream. *Proc. R. Soc. Math. Phys. Eng. Sci.*
427 **174**, 322–338 (1940).
- 428 46. Zingg, T. Beitrag zur Schotteranalyse. (1935).

- 429 47. Barrett, P. J. The shape of rock particles, a critical review. *Sedimentology* **27**, 291–303 (1980).
- 430 48. Blott, S. J. & Pye, K. Particle shape: a review and new methods of characterization and
431 classification. *Sedimentology* **55**, 31–63 (2008).
- 432 49. Domokos, G., Sipos, A., Szabó, T. & Várkonyi, P. Pebbles, Shapes, and Equilibria. *Math. Geosci.*
433 **42**, 29–47 (2009).
- 434 50. Szabó, T. & Domokos, G. A new classification system for pebble and crystal shapes based on
435 static equilibrium points. *Cent. Eur. Geol.* **53**, 1–19 (2010).
- 436 51. Domokos, G., Kun, F., Sipos, A. Á. & Szabó, T. Universality of fragment shapes. *Sci. Rep.* **5**, (2015).
- 437 52. Novák-Szabó, T. *et al.* Universal characteristics of particle shape evolution by bed-load chipping.
438 *Sci. Adv.* **4**, eaao4946 (2018).
- 439 53. Oakey, R. J. *et al.* Grain-Shape Analysis--A New Method for Determining Representative Particle
440 Shapes for Populations of Natural Grains. *J. Sediment. Res.* **75**, 1065–1073 (2005).
- 441 54. Cassel, M., Piégay, H. & Lavé, J. Effects of transport and insertion of radio frequency
442 identification (RFID) transponders on resistance and shape of natural and synthetic pebbles:
443 applications for riverine and coastal bedload tracking: Transport and Rfid-Insertion Effects on the
444 Fragility of Pebbles. *Earth Surf. Process. Landf.* (2016) doi:10.1002/esp.3989.
- 445 55. Attal, M., Lave, J. & Masson, J. P. New Facility to Study River Abrasion Processes. *J. Hydraul. Eng.*
446 **132**, 624–628 (2006).
- 447 56. Attal, M. & Lavé, J. Pebble abrasion during fluvial transport: Experimental results and
448 implications for the evolution of the sediment load along rivers. *J. Geophys. Res.* **114**, (2009).
- 449 57. Cassel, M. *et al.* Evaluating a 2D image-based computerized approach for measuring riverine
450 pebble roundness. *Geomorphology* (2018) doi:10.1016/j.geomorph.2018.03.020.
- 451 58. Chapuis, M., Bright, C. J., Hufnagel, J. & MacVicar, B. Detection ranges and uncertainty of passive
452 Radio Frequency Identification (RFID) transponders for sediment tracking in gravel rivers and
453 coastal environments. *Earth Surf. Process. Landf.* **39**, 2109–2120 (2014).

- 454 59. Arnaud, F., Piégay, H., Vaudor, L., Bultingaire, L. & Fantino, G. Technical specifications of low-
455 frequency radio identification bedload tracking from field experiments: Differences in antennas,
456 tags and operators. *Geomorphology* **238**, 37–46 (2015).
- 457 60. Haschenburger, J. K. & Church, M. Bed material transport estimated from the virtual velocity of
458 sediment. *Earth Surf. Process. Landf.* **23**, 791–808 (1998).
- 459 61. Cecchetto, M. *et al.* Diffusive Regimes of the Motion of Bed Load Particles in Open Channel Flows
460 at Low Transport Stages. *Water Resour. Res.* **54**, 8674–8691 (2018).
- 461 62. Ballio, F., Radice, A., Fathel, S. L. & Furbish, D. J. Experimental Censorship of Bed Load Particle
462 Motions and Bias Correction of the Associated Frequency Distributions. *J. Geophys. Res. Earth*
463 *Surf.* **124**, 116–136 (2019).
- 464 63. Auel, C., Albayrak, I., Sumi, T. & Boes, R. M. Sediment transport in high-speed flows over a fixed
465 bed: 1. Particle dynamics. *Earth Surf. Process. Landf.* **42**, 1365–1383 (2017).
- 466 64. Demir, T. The influence of particle shape on bedload transport in coarse-bed river channels.
467 (Durham University, 2000).
- 468 65. Bridge, J. S. & Bennett, S. J. A model for the entrainment and transport of sediment grains of
469 mixed sizes, shapes, and densities. *Water Resour. Res.* **28**, 337–363 (1992).
- 470 66. Bagnold, R. A. *An approach to the sediment transport problem from general physics.*
471 <http://pubs.er.usgs.gov/publication/pp4221> (1966).
- 472 67. Parker, G., Klingeman, P. C. & McLean, D. G. BEDLOAD AND SIZE DISTRIBUTION IN PAVED
473 GRAVEL-BED STREAMS. *ASCE J Hydraul Div* **108**, 544–571 (1982).
- 474 68. Wilcock, P. R. & Crowe, J. C. Surface-based Transport Model for Mixed-Size Sediment. *J. Hydraul.*
475 *Eng.* **129**, 120–128 (2003).
- 476 69. Sneed, E. D. & Folk, R. L. Pebbles in the Lower Colorado River, Texas a Study in Particle
477 Morphogenesis. *J. Geol.* **66**, 114–150 (1958).
- 478
- 479

480 **Author contributions**

481 M.C., H.P., and J.L. contributed to the design of the experiment. M.C., J.L., and H.P. analyzed
482 experimental results; J.L., H.P., M.C., A.R., and J-R.M. wrote the manuscript.

483

484 **Corresponding author**

485 Correspondence to Mathieu Cassel.

486

487 **Competing Interests**

488 The authors declare no competing interests.